

**To,**

**Editor – Climates of the Past**

We would like to thank the editor and the reviewers for their comments. Our primary intent with this paper, as described in the introduction, is to report on the differing response of symmetric versus asymmetric geographies to orbital forcing. We acknowledge that this first step is indeed mainly descriptive and does not provide a detailed dynamical analysis of the Land Asymmetry Effect. We reiterate that this study (saving monthly mean GCM output) was never intended to be a detailed dynamical examination of the climatic response to changing geographies under different orbits and that's way beyond the scope of the paper. However, we do observe interesting patterns related to clouds, snow cover, cross-equator sea-level pressure (wind) pattern that impacts sea ice, etc. which then amplifies the response. However, these interesting patterns require additional study, and we hope some well-designed dynamical experiments could be conducted to tease out physical mechanisms behind the correlations in the future.

We hope the editor views this manuscript as simply a first step, reporting on interesting GCM results that use a unique geographic set up to illustrate that there are far field influences of global geography that moderate/accentuate the Earth's response to orbital forcing.

Thanking you,

Rajarshi Roychowdhury, Rob DeConto

## Response to Review #1:

The authors made significant efforts to attempt to respond to the requests of the reviewers. They must be praised for that. Nevertheless this does not seem fully satisfactory to me since some of the important requests are rejected as 'irrelevant' (which I can partially understand) or worse, the additional parts add more confusion. The section about the clouds, the liquid water content, atmospheric pressure, snow cover and sea ice should inform the reader about the feedbacks but this is not really the case. Firstly, the analysis is almost exclusively limited to correlations and, on the other hand, it lacks an explanation of what the variables really are (is it annual average, seasonal, other?) and what is the physics behind the correlation.

The GCM simulations used for this study are relatively coarse resolution and only saved select meteorological fields as time averaged (monthly means). The output is not suitable to exploring some atmospheric dynamical processes that would be interesting to explore in the context of the LAE patterns, limiting us with few select examples of meteorological fields that relate with the observed LAE. These include clouds, snow cover, and sea ice, which provide a strong regional (radiative) amplifying or dampening effect of local orbital forcing. We have extended our analysis based on these variables, and have added the explanation of the variables used in the figures.

The authors wrote themselves that a 'true discussion' of the role of asymmetry would involve simulations at every possible orbital configuration, including all possible eccentricity values'. And it really puzzles me because they have only 6 experiments, all with the same eccentricity. We are really far from covering the whole field of orbital parameters (and I understand that it is impossible for a GCM). However, what is done here is probably statistically not significant. Moreover, 'statistical methods' (latin hypercube) are very efficient to identify the set of variables that would be more representative for the full ranges of combinations although, even a carefully designed set of experiments would mean too many experiments.

The aim of this first paper was to point out that the Land Asymmetry Effect exists, and we extend the results to show that the LAE is different at various orbital configurations. As mentioned above, it is impossible to cover the entire orbital range using a GCM. Choosing a set of orbital parameters is also impractical, as any one combination of orbital parameters will not be representative of the orbital range. For phenomena that depend strongly on the correlation of two or more variables, Latin hypercube sampling has little advantage over traditional Monte Carlo sampling. And being limited by computational resources, we cannot run an extremely high number of orbital combinations. Thus, we chose a different approach to run the simulations at highest and lowest obliquity, and 4 precessional configurations. We choose the mean value of eccentricity, which is the most frequent value of eccentricity in the last 2.0 million years. The value of eccentricity (0.034) is chosen from the plot of the kernel density estimate of the eccentricity values from the last 2.0 million years.

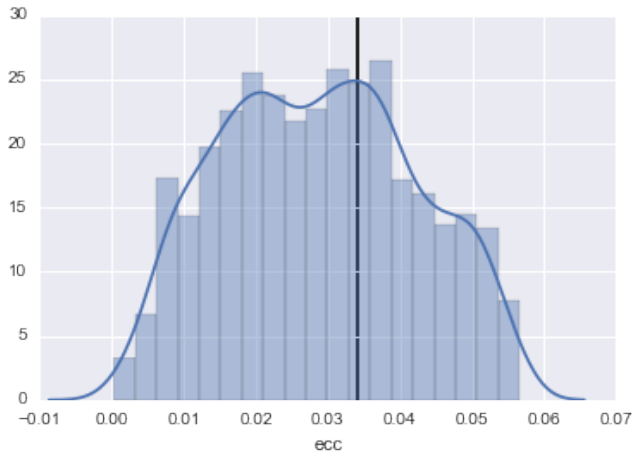


Figure: KDE Distribution plot of the Eccentricity values from the last 2.0 million years. The selected value of eccentricity (0.034) is shown by the black vertical line.

## Response to Review #2:

1 – Quite generally, this paper still falls short of my expectations in terms of result analysis. It is quite frustrating to see interesting model results without any explanation of the physical processes involved. Compared to the previous version, the authors are now presenting correlations with some key variables. This might be a first step, but the manuscript still remains quite descriptive on this part.

The GCM simulations used for this study are relatively coarse resolution and only saved select meteorological fields as time averaged (monthly means). The output is not suitable to exploring some atmospheric dynamical processes that would be interesting to explore in the context of the LAE patterns, limiting us with few select examples of meteorological fields that relate with the observed LAE. These include clouds, snow cover, and sea ice, which provide a strong regional (radiative) amplifying or dampening effect of local orbital forcing. We have extended our analysis based on these variables, along with the physical processes involved.

2 – Slab ocean. I do very well understand that a slab ocean is computationally more efficient : My comments did not concern the use of a slab ocean in this study, but the discussion of its impact on the results. Is the parameterized ocean heat flux symmetric when temperatures and continents are symmetric? If so, then it should be explained clearly in the text. If not, this might be a serious problem.

Yes, the parameterized ocean heat flux is symmetric in our symmetrical Earth simulations. Poleward oceanic heat flux is defined as a function of the temperature gradient and the zonal fraction of land and sea at given latitude in the model. In the model, the ocean heat flux parameterization is based only on observed estimates. This allows the model to be used for paleoclimatic applications with very different ocean configurations than the present. (Thompson and Pollard, 1997). A description of ocean heat transport symmetry is now included in the manuscript.

Thompson, S. L. and Pollard, D.: Greenland and Antarctic Mass Balances for Present and Doubled Atmospheric CO<sub>2</sub> from the GENESIS Version-2 Global Climate Model, *J. Clim.*, 10(5), 871–900, 1997.

1 **Interhemispheric Effect of Global Geography on Earth's Climate Response to**  
2 **Orbital Forcing**

3 **Rajarshi Roychowdhury<sup>1</sup> and Robert DeConto<sup>1</sup>**

4 <sup>1</sup>University of Massachusetts - Amherst

5 *Correspondence to:* [rroychowdhur@geo.umass.edu](mailto:rroychowdhur@geo.umass.edu)

6 **Postal Address:**

7 Department of Geosciences

8 627 North Pleasant Street

9 233 Morrill Science Center

10 University of Massachusetts

11 Amherst, MA 01003-9297

12

13 **Abstract**

14 The climate response of the Earth to orbital forcing shows a distinct hemispheric asymmetry due  
15 to the unequal distribution of land in the Northern versus Southern Hemispheres. This  
16 asymmetry is examined using a Global Climate Model (GCM) for different climate responses  
17 such as Mean Summer Temperatures and Positive Degree Days. A Land Asymmetry Effect  
18 (LAE) is quantified for each hemisphere and the results show how changes in obliquity and  
19 precession translate into variations in the calculated LAE. We find that the global climate  
20 response to specific past orbits is likely unique and modified by complex climate-ocean-

21 cryosphere interactions that remain poorly known. Nonetheless, these results provide a baseline  
22 for interpreting contemporaneous proxy climate data spanning a broad range of latitudes, which  
23 maybe useful in paleoclimate data-model comparisons, and individual time-continuous records  
24 exhibiting orbital cyclicality.

## 25 **1. Introduction**

26 The arrangement of continents on the Earth's surface plays a fundamental role in the Earth's  
27 climate response to forcing. Due to the asymmetric global geography of the Earth, more  
28 continental land area is found in the Northern Hemisphere (68%) as compared to the Southern  
29 Hemisphere (32%). These different ratios of land vs. ocean in each hemisphere affect the balance  
30 of incoming and outgoing radiation, atmospheric circulation, ocean currents, and the availability  
31 of terrain suitable for growing glaciers and ice-sheets. Subsequently, the climate response of the  
32 Earth to radiative forcing is asymmetric (Figure 1b and 1c), while the radiative forcing (top-of-  
33 atmosphere solar radiation) itself is symmetric across the two hemispheres (Figure 1a). As a  
34 result of the inherent land-ocean asymmetry of the Earth, the climatic responses of the Northern  
35 and Southern Hemisphere differ for an identical change in radiative forcing (Barron et al., 1984;  
36 Deconto et al., 2008; Kang et al., 2014; Short et al., 1991).

37 Charles Lyell was the first to consider the influence of paleogeography on surface temperatures,  
38 in the context of the connection between climate and the modern distribution of land and sea  
39 (Lyell, 1832). By comparing the climates of the Northern and Southern Hemispheres and the  
40 distribution of land and sea, Lyell pointed out that the present continental distribution lowers  
41 high latitude temperatures in both hemispheres. He further pointed out that dominance of ocean  
42 in the Southern Hemisphere leads to mild winters and cool summers. Lyell's work is significant

43 in the context of this paper, because it first sparked the debate of continental forcing versus  
44 astronomical forcing of climate.

45 Since then, a number of classic studies have shown interhemispheric asymmetry in climate  
46 response of Northern and Southern Hemispheres. Climate simulations made with coupled  
47 atmosphere-ocean GCMs typically show a strong asymmetric response to greenhouse-gas  
48 loading, with Northern Hemisphere high latitudes experiencing increased warming compared to  
49 Southern Hemisphere high latitudes (Flato and Boer, 2001; Stouffer et al., 1989). GCMs also  
50 show that the Northern and Southern Hemispheres respond differently to changes in orbital  
51 forcing (e.g. Philander et al., 1996). While the magnitude of insolation changes through each  
52 orbital cycle is identical for both hemispheres, the difference in climatic response can be  
53 attributed to the fact that Northern Hemisphere is land-dominated while Southern Hemisphere is  
54 water dominated (Croll, 1870). This results in a stronger response to orbital forcing in the  
55 Northern Hemisphere relative to the Southern Hemisphere.

56 The distribution of continents and oceans have an important effect on the spatial heterogeneity of  
57 the Earth's energy balance, primarily via the differences in albedos and thermal properties of  
58 land versus ocean (Trenberth et al., 2009). The latitudinal distribution of land has a dominant  
59 effect on zonally averaged net radiation balance due to its influence on planetary albedo and  
60 ability to transfer energy to the atmosphere through long-wave radiation, and fluxes of sensible  
61 and latent heat. The latitudinal net radiation gradient controls the total poleward heat transport  
62 requirement, which is the ultimate driver of winds, and ocean circulation (Stone, 1978). Oceans  
63 have a relatively slower response to seasonal changes in insolation due to the higher specific heat  
64 of water as compared to land, and mixing in the upper ~10-150 m of the ocean. As a result, in the  
65 ocean-dominated Southern Hemisphere, the surface waters suppress extreme temperature swings

66 in the winter and provide the atmosphere with a source of moisture and diabatic heating. In the  
67 land-dominated Northern Hemisphere, the lower heat capacity of the land combined with  
68 relatively high albedo results in greater seasonality, particularly in the interiors of large  
69 continents of Asia and North America. The land surface available in a particular hemisphere  
70 also affects the potential for widespread glaciation, and the extreme cold winters associated with  
71 large continents covered by winter snow.

72 Continental geography has a strong impact on polar climates, as is evident from the very  
73 different climatic regimes of the Arctic and the Antarctic. Several early paleoclimate modeling  
74 studies using GCMs investigated continental distribution as a forcing factor of global climate  
75 (e.g. Barron et al., 1984; Hay et al., 1990). These studies demonstrated that an Earth with its  
76 continents concentrated in the low latitudes is warmer and has lower equator-to-pole temperature  
77 gradients than an Earth with only polar continents. Although these early model simulations did  
78 not incorporate all the complexities of the climate system, the results provided valuable insights  
79 from comparative studies of polar versus equatorial continents in the Earth and showed that  
80 changes in continental configuration has significant influence on climatic response to forcing.

81 The asymmetry in the climates of the Northern and Southern Hemispheres can be attributed to  
82 three primary causes: (i) Astronomical: Variation in insolation intensity across the Northern and  
83 Southern Hemispheres caused by the precession of the equinoxes (today perihelion coincides  
84 with January 3, just after the December 21 solstice, leading to slightly stronger summer  
85 insolation in the Southern Hemisphere); (ii) Continental geography: the effect of the continental  
86 geography on climate as described above; and (iii) Interhemispheric continental geography, i.e.  
87 the effect of Northern Hemisphere continental geography on Southern Hemisphere climate and  
88 vice-versa. The aim of this study is to gain a better understanding and isolate the effect of



89 interhemispheric continental geography on climate by comparing results from GCM simulations  
90 using modern versus idealized (hemispherically symmetric) global geographies. The GCM  
91 simulations with modern and idealized (symmetric) geographies are used to quantify the  
92 different climate responses to a range of orbits. By comparing the climatic response from  
93 simulations with different geographies, we isolate and estimate the effect of interhemispheric  
94 continental geography, i.e. the influence of one hemisphere's geography on the climate response  
95 of the opposite hemisphere.

96 One of the main caveats of this study is the lack of a dynamical ocean in our model setup. While  
97 this presents certain limitations, the model's computational efficiency has the advantage of  
98 allowing a wide range of orbital parameter space to be explored. We view the inclusion of a full  
99 depth dynamical ocean as a next step, hopefully motivated in part by the results published here.  
100 Furthermore, dynamical ocean models introduce an additional level of complexity and model-  
101 dependencies that we think are best avoided in this initial study.

## 102 **2. Model**

### 103 **2.1 Experimental design**

104 General Circulation Models (GCM) have been used extensively to study the importance of  
105 geography on the Earth's climate in the past. In this study, we use the latest (2012) version of the  
106 Global ENvironmental and Ecological Simulation of Interactive Systems (GENESIS) 3.0 GCM  
107 with a slab ocean component (Thompson and Pollard, 1997) rather than a full-depth dynamical  
108 ocean (Alder et al., 2011). The slab-ocean predicts sea surface temperatures and ocean heat  
109 transport as a function of the local temperature gradient and the zonal fraction of land versus sea  
110 at each latitude. While explicit changes in ocean currents and the deep ocean are not represented,

111 the computational efficiency of the slab-ocean version of the GCM allows numerous simulations  
112 with idealized global geographies and greatly simplifies interpretations of the sensitivity tests by  
113 precluding complications associated with ocean model dependencies. The ocean depth is limited  
114 to 50-m (enough to capture the seasonal cycle of the mixed layer). In addition to the atmosphere  
115 and slab-ocean, the GCM includes model components representing vegetation, soil, snow, and  
116 thermo-dynamic sea ice. The 3-D atmospheric component of the GCM uses an adapted version  
117 of the NCAR CCM3 solar and thermal infrared radiation code (Kiehl et al., 1998) and is coupled  
118 to the surface components by a land-surface-transfer scheme. In the setup used here, the model  
119 atmosphere has a spectral resolution of T31 ( $\sim 3.75^\circ$ ) with 18 vertical layers. Land-surface  
120 components are discretized on a higher resolution  $2^\circ \times 2^\circ$  grid.

121 The GCM uses various geographical boundary conditions (described below) in  $2^\circ \times 2^\circ$  and  
122 spectral T31 grids for surface and AGCM models, respectively. For each set of experiments, the  
123 model is run for 50 years. Spin-up is taken into account, and equilibrium is effectively reached  
124 after about 20 years of integration. The results used to calculate interhemispheric effects are  
125 averaged over the last 20 years of each simulation. Greenhouse gas mixing ratios are identical in  
126 all experiments and set at preindustrial levels with  $\text{CO}_2$  set at 280 ppmv,  $\text{N}_2\text{O}$  at 288 ppbv and  
127  $\text{CH}_4$  at 800 ppbv. The default values for  $\text{CFCl}_3$  and  $\text{CF}_2\text{Cl}_2$  values are set at 0 ppm. The solar  
128 constant is maintained at  $1367 \text{ Wm}^{-2}$ .

## 129 **2.2 Asymmetric and symmetric Earth geographies**

130 The GCM experiments are divided into three sets: 1) Preindustrial CONTROL 2) NORTH-  
131 SYMM and 3) SOUTH-SYMM. The Preindustrial CONTROL experiments use a modern global  
132 geography spatially interpolated to the model's  $2^\circ \times 2^\circ$  surface grid (Koenig et al., 2012). The

133 geography provides the land-ice sheet-ocean mask and land–surface elevations used by the  
134 GCM.

135 To simulate the climate of an Earth with meridionally symmetric geographies, we created two  
136 sets of land surface boundary conditions: NORTH-SYMM and SOUTH-SYMM. For the  
137 NORTH-SYMM experiments, the CONTROL experiment boundary conditions are used to  
138 generate a modified GCM surface mask, by reflecting the Northern Hemisphere geography  
139 (land-sea-ice mask, topography, vegetation, soil texture) across the equator into the Southern  
140 Hemisphere. Similarly, in the experiment SOUTH-SYMM, the land mask and geographic  
141 boundary conditions in the Southern Hemisphere are mirrored in the Northern Hemisphere. The  
142 NORTH-SYMM and SOUTH-SYMM boundary conditions are shown in Figure 2b and 2c, with  
143 the CONTROL (Figure 2a) for comparison. Poleward oceanic heat flux is defined as a function  
144 of the temperature gradient and the zonal fraction of land and sea at given latitude in the model;  
145 hence the parameterized ocean heat flux is symmetric in our symmetrical Earth simulations.

### 146 **3. Symmetry (and asymmetry in GCM results)**

147 In the first experimental setup, we run the GCM with modern day orbital configuration, i.e.  
148 eccentricity is set at 0.0167, obliquity is set at  $23.5^\circ$  and precession such that perihelion  
149 coincides with Southern Hemisphere summer. The radiation at Top-of-Atmosphere is symmetric  
150 across both Hemispheres (Figure 3a and 3b). Mean Summer Temperature (ST) is calculated from  
151 the GCM as the mean of the average daily temperatures for the summer months in each  
152 hemisphere. We define summer by an insolation threshold ( $325 \text{ W/m}^2$ ); which accounts for the  
153 astronomical positions as well as the phasing of the seasonal cycle of insolation. The zonal  
154 averages of ST (calculated at each latitude) demonstrate the inherent asymmetry in the Earth's  
155 climate between Northern and Southern Hemispheres, especially evident in the higher latitudes

156 (Figure 3c). Positive Degree Days (PDD) captures the intensity as well as the duration of the  
157 melt season, and has been shown to be indicative of ice-sheet response to changes in external  
158 forcing. Figure 3d shows the PDD for modern orbit, with zonal averages plotted in the log scale.  
159 The asymmetry between the Northern and Southern Hemispheres is captured by the GCM in the  
160 calculated PDDs.

161 Next, we maintain the modern orbit to test the effect of meridionally symmetric continents  
162 (Figure 3e-h). Figure 3e and 3f show ST and PDD from a simulation in which the Northern  
163 Hemisphere geography is reflected in the Southern Hemisphere (thus making the Earth  
164 geographically symmetric). Figure 3g and Figure 3h show ST and PDD from the simulation with  
165 symmetric Southern Hemisphere continents. Symmetric continents make the climates of  
166 Northern and Southern Hemispheres symmetric (>95%). However, due to the current timing of  
167 perihelion with respect to the summer solstices, there remains some minor asymmetry. Using an  
168 orbit in which perihelion coincides with equinoxes will make the climate truly symmetrical.

## 169 **4. Modern Orbit Simulations**

### 170 **4.1 Effect of Southern Hemisphere (SH) on Northern Hemisphere (NH) climate**

171 To estimate the effect of SH continental geography on NH climate, we subtract the NH climate  
172 of the NORTH-SYMM simulation (symmetric Northern continents in both hemispheres) from  
173 the CONTROL simulation (asymmetric, modern orbit). In these two simulations, the only  
174 difference in setup is the Southern Hemispheric continental distribution. Thus the difference in  
175 NH climate from the two simulations, if any, can be safely ascribed as the effect of SH  
176 continental geography on NH climate. We quantify this interhemispheric effect for ST (for NH)  
177 as:

178 
$$e_{\widehat{Summer\ Temp}} = \frac{1}{n} \sum_i^n (T_i^{control} - T_i^{north}) \quad \dots(1)$$

179 Analogous to the effect for ST, the effect for PDD, which we call the “Land Asymmetry Effect”  
 180 (LAE), is defined as follows:

181 
$$LAE_{(NH)} = PDD^{control} - PDD^{north} \quad \dots(2)$$

182 Where  $T_i^{control}$  and  $PDD^{control}$  are the mean daily temperature and PDD from the CONTROL  
 183 simulation, and  $T_i^{North}$  and  $PDD^{North}$  are the mean daily temperature and PDD from the simulation  
 184 with the North-symmetric geography (NORTH-SYMM). ‘n’ is the number of days in the  
 185 summer months in each hemisphere.

186 **4.2 Effect of Northern Hemisphere (NH) on Southern Hemisphere (SH) climate**

187 Similarly, we estimate the effect of NH continental geography on the SH by subtracting the SH  
 188 climate of the SOUTH-SYMM simulation (symmetric southern continents in both hemispheres)  
 189 from the CONTROL simulation (asymmetric, modern orbit). In these two simulations, the  
 190 differences in SH climate in the CONTROL and SOUTH-SYMM simulations, if any, can be  
 191 ascribed as the ‘effect of NH continental geography on SH climate’. We quantify this  
 192 interhemispheric effect for ST (for SH) and the LAE as:

193 
$$e_{\widehat{Summer\ Temp}} = \frac{1}{n} \sum_i^n (T_i^{control} - T_i^{south}) \quad \dots(3)$$

194 
$$LAE_{SH} = PDD^{control} - PDD^{south} \quad \dots(4)$$

195 where  $T_i^{\text{control}}$  and  $\text{PDD}^{\text{control}}$  are the mean daily temperature and PDD from the CONTROL  
196 simulation, and  $T_i^{\text{south}}$  and  $\text{PDD}^{\text{south}}$  are the mean daily temperature and PDD from the simulation  
197 with the south-symmetric geography (SOUTH-SYMM).

### 198 **4.3 Results of Modern Orbit Simulations**

199 Figure 4a and 4b show the interhemispheric effect of continental geography on ST and PDD  
200 respectively. For the Northern Hemisphere, the summer temperatures are calculated when the  
201 insolation intensity over the Northern Hemisphere is strongest. The asymmetry in the Southern  
202 Hemisphere landmasses leads to weakening of the summer warming over North America and  
203 Eurasia (blue shaded regions correspond to cooling). Consequently, summer temperatures over  
204 Northern Hemisphere continents are lower by 3-6°C relative to a symmetric Earth. There is a  
205 positive warming effect in the North-Atlantic Ocean, and in general the Northern Hemisphere  
206 oceans are slightly warmer relative to a symmetric Earth. The general trends in the  
207 interhemispheric effect on PDD (LAE) (Figure 4b) mimic those of the summer temperatures  
208 (Figure 4a).

209 For the Southern Hemisphere, the summer temperatures are calculated when the insolation is  
210 most intense over the Southern Hemisphere during the year. Southern Hemisphere landmasses,  
211 except Antarctica, generally show a cooling response during summer, due to Northern  
212 Hemisphere geography. Over Antarctica, summer temperatures are higher in the control  
213 simulations than in the symmetric simulations, leading to the inference that there is a warming  
214 (increase) in summer temperatures due to interhemispheric effect. Also, the Southern Ocean  
215 shows a strong positive temperature effect (warming) relative to a symmetric Earth, although this  
216 Southern Ocean response might be different or modified if a full-depth dynamical ocean model  
217 were used.

## 218 5. Idealized Orbit Simulations

219 Next, we examine the effect of the opposite hemisphere on the Earth's climate response at  
220 extreme obliquities (axial tilt) and idealized precessional configurations (positions of the  
221 solstices and equinoxes in relation to the eccentric orbit). The orbital parameters used in these  
222 experiments are idealized and do not correspond to a specific time in Earth's history. Rather,  
223 they are chosen to provide a useful framework for studying the Earth's climate response to  
224 precession and obliquity. HIGH and LOW orbits approximate the highest and lowest obliquity in  
225 the last three million years (Berger and Loutre, 1991). NHSP (Northern Hemisphere Summer at  
226 Perihelion) and SHSP (Southern Hemisphere Summer at Perihelion) orbits correspond to  
227 Northern and austral summers coinciding with perihelion, respectively. The other two  
228 precessional configurations considered are EP1 and EP2, with the perihelion coinciding with the  
229 equinoxes. For the idealized precession simulations, the obliquity is set at its mean value  
230 averaged over the last 3 million years. Eccentricity is set at the same moderate value (mean  
231 eccentricity over the last 3 million years) for all simulations. Table 1 summarizes the orbits used  
232 in the ensemble of model simulations. Here, we focus only on the LAE, as PDD is a better  
233 indicator of air temperature's influence on annual ablation over ice-sheets than summer  
234 temperature, since this metric captures both the intensity and duration of the melt season.

235 Changes in precession primarily affect seasonal insolation intensity that is well known to be out-  
236 of-phase in both hemispheres (Lyell, 1832). To demonstrate an asymmetry in the climate  
237 response to precession, we take the differences between two arbitrarily chosen extremes in the  
238 precession cycle (NHSP and SHSP) for both the forcing and the climate response. The forcing  
239 (summer energy (J)) calculated at the top of the atmosphere is symmetric across both  
240 hemispheres (Figure 5a). The difference in the PDDs ( $\Delta\text{PDD}_{\text{precession}}$ ) is the Earth's climate

241 response to the combined effect of the two precessional motions (wobbling of the axis of rotation  
242 and the slow turning of the orbital ellipse). The climate response ( $\Delta PDD_{\text{precession}}$ ) is asymmetric  
243 across both hemispheres (Figure 5b). However, when we run the precessional simulations in a  
244 Earth with symmetric continents, the climate response to precession is symmetrical (Figure 5c  
245 and 5d).

246 In contrast to precession, obliquity alters the seasonality of insolation equally in both  
247 hemispheres (Figure 5e). A reduction in the tilt from  $24.5^\circ$  (HIGH) to  $22^\circ$  (LOW) reduces  
248 annual insolation by  $\sim 17 \text{ W/m}^2$  and summer insolation by  $\sim 45 \text{ W/m}^2$  in the high latitudes. In the  
249 tropics, summer insolation increases by up to  $\sim 5 \text{ W/m}^2$ . Loutre et al. (2004) among others  
250 predicted that global ice volume changes at the obliquity periods could be interpreted as a  
251 response to mean annual insolation and meridional insolation gradients. To demonstrate  
252 asymmetry in the climate response to obliquity, we take the differences between the highest and  
253 lowest obliquities for both the forcing and the climate response. The difference in the PDDs  
254 ( $\Delta PDD_{\text{obliquity}}$ ) is the Earth's climate response to changes in tilt. Figure 5f shows  $\Delta PDD_{\text{obliquity}}$   
255 and the zonal averages reveal the asymmetry in the obliquity climate response. The same  
256 simulations with North-symmetric Earth (Figure 5g) and South-symmetric Earth (Figure 5h)  
257 produce symmetrical climate responses to the obliquity cycle.

## 258 **5. Results of Idealized Orbit Simulations**

259 The effect of SH continental geography on NH at the idealized orbits is estimated using the same  
260 method described above, with the LAE for a given orbit (for NH) calculated as:

$$261 \quad LAE_{(NH)} = PDD_{\text{orbit}}^{\text{control}} - PDD_{\text{orbit}}^{\text{north}} \quad \dots(5)$$



262 Similarly, the effect of NH continental geography on SH at the idealized orbits is estimated using  
263 the same method described above, with the LAE for a given orbit (for SH) calculated as:

$$264 \quad LAE_{(SH)} = PDD_{orbit}^{control} - PDD_{orbit}^{south} \quad \dots(6)$$

265 Figure 6a shows the spatial variation of LAE when perihelion coincides with Northern  
266 Hemisphere summer (NHSP). The Northern Hemisphere landmasses show a strong negative  
267 response. In this orbit, the Northern Hemisphere experiences elevated summer insolation, but the  
268 response is attenuated by the interhemispheric effect. This dampening effect is greatest in the  
269 interiors of the Northern Hemisphere continents. If precession is considered in isolation (i.e.  
270 constant obliquity), according to the astronomical theory of climate the Northern Hemisphere  
271 should experience ‘interglacial’ conditions when perihelion coincides with boreal summer.  
272 However, because of the interhemispheric effect, interglacial (warm summer) conditions are  
273 muted relative to those on a symmetric Earth. During this orbit, the Southern Hemisphere  
274 experiences ‘glacial’ (cold summer) conditions due to the weaker summer insolation. The  
275 positive effect in the Southern Hemisphere leads to weaker cooling relative to a symmetric Earth.  
276 Thus, when perihelion coincides with Northern Hemisphere summer, the interhemispheric effect  
277 dampens the magnitude of ‘glacial’ versus ‘interglacial’ conditions in both hemispheres.

278 Figure 6b shows the spatial variation of LAE when perihelion coincides with Southern  
279 Hemisphere summer (SHSP). The Northern Hemisphere continents have a weak positive effect,  
280 leading to slightly warmer conditions relative to a symmetric Earth. In this orbit, the southern  
281 high latitudes experience intense summer insolation. The positive warming effect amplifies the  
282 already warm conditions in the Southern Hemisphere. Figures 6c and 6d show the spatial  
283 variation of LAE at the two equinoxes respectively, i.e. when Northern Hemisphere vernal

284 equinox is at perihelion (EP1) and when Northern Hemisphere autumnal equinox is at perihelion  
285 (EP2). The LAE is in general weaker at the equinoxes than at the solstices.

286 At HIGH obliquity, there exists a negative effect on Northern Hemisphere continents (Figure  
287 6e), which mutes the strong insolation intensity during summer months. In the Northern  
288 Hemisphere, as a result of continental asymmetry, a decrease in the equator to pole temperature  
289 gradient is observed. A lowering of summer temperatures and temperature gradient due to the  
290 interhemispheric effect has a negative impact on the deglaciation trigger associated with HIGH  
291 obliquity orbits. Thus the interhemispheric effect would hinder the melting of ice during high-  
292 obliquity orbits. In the Southern Hemisphere, the positive interhemispheric effect on PDD over  
293 Antarctica and the Southern Ocean leads to overall higher temperatures in the high southern  
294 latitudes as compared to a symmetric Earth. Thus, during the high obliquity orbits, positive effect  
295 helps deglaciation.

296 At LOW obliquity, the negative effect over Northern Hemisphere continents is generally less  
297 intense (Figure 6f). However, even the modest lowering of summer temperatures caused by the  
298 interhemispheric effect would support the growth of ice sheets during low obliquity orbits. The  
299 positive effect (warming) in the high Southern latitudes would delay the growth of ice sheets.

## 300 **6. LAE for orbital cycles**

301 Next, we calculate the LAE for a transition through a precessional cycle. We take two arbitrary  
302 end points in the precessional cycle (NHSP and SHSP), and calculate the difference of PDDs  
303 between the two simulations ( $\Delta PDD_{precession\_cycle}$ ). The LAE for precessional cycle is therefore  
304 calculated as:

$$305 \quad LAE_{(NH)} = \Delta PDD_{precession\_cycle}^{control} - \Delta PDD_{precession\_cycle}^{north} \quad \dots(7)$$

$$306 \quad LAE_{(SH)} = \Delta PDD_{precession\_cycle}^{control} - \Delta PDD_{precession\_cycle}^{south} \quad \dots(8)$$

307 The LAE shows a strong negative effect in the Northern Hemisphere (Figure 7a). For the  
 308 Northern Hemisphere, this transition from SHSP to NHSP equates to a transition from cool to  
 309 warm climate. The negative interhemispheric effect decreases the  $\Delta PDD$  in the real Earth, thus  
 310 weakening the effect of precession in the Northern Hemisphere. The Southern Hemisphere  
 311 shows a positive effect on PDD at high latitudes. For the Southern Hemisphere, the transition  
 312 from SHSP to NHSP equates to a transition from warmer to cooler climate. The positive  
 313 interhemispheric effect at high latitudes decreases the  $|\Delta PDD|$  in the real Earth, thus weakening  
 314 the effect of precessional cycle in the Southern Hemisphere high latitudes.

315 To calculate the LAE for a transition through the obliquity cycle, we take the highest and lowest  
 316 obliquities (HIGH and LOW), and calculate the difference of PDDs between the two simulations  
 317 ( $\Delta PDD_{obliquity\_cycle}$ ). ). The LAE for obliquity cycle is therefore calculated as:

$$318 \quad LAE_{(NH)} = \Delta PDD_{obliquity\_cycle}^{control} - \Delta PDD_{obliquity\_cycle}^{north} \quad \dots(9)$$

$$319 \quad LAE_{(SH)} = \Delta PDD_{obliquity\_cycle}^{control} - \Delta PDD_{obliquity\_cycle}^{south} \quad \dots(10)$$

320 The Northern Hemisphere shows a small negative effect in the high latitudes, and a positive  
 321 effect in the low latitudes (Figure 7b). The transition from LOW to HIGH corresponds to a  
 322 transition from cold to warm climate. The negative interhemispheric effect decreases the  $\Delta PDD$ ,  
 323 thus weakening the climate response of obliquity cycle in the high latitudes. The positive  
 324 interhemispheric effect increases the  $\Delta PDD$ , thus strengthening the climate response of obliquity  
 325 cycle in the low latitudes in the Northern Hemisphere. The Southern Hemisphere shows largely a  
 326 negative effect, with a positive effect in the high latitudes. The transition from LOW to HIGH

327 corresponds to a transition from cold to warm climate. The positive interhemispheric effect  
328 increases the  $\Delta$ PDD, thus amplifying the effect of obliquity over Antarctica.

## 329 **6. Impact of various climatological variables on LAE**

330 A comprehensive, mechanistic evaluation of the hemispheric effect is beyond the scope of this  
331 initial study. However, as a first step, we test the relationship between the hemispheric LAE and  
332 various atmospheric processes by exploring correlations between the inter hemispheric responses  
333 to orbital forcing, and climatological fields related to changes in radiation (clouds), dynamics  
334 (heat and moisture convergence), and feedbacks related to surface processes (sea ice and snow  
335 albedo).

336 Numerous studies have shown the impact of variation in distribution of clouds (e.g., Meleshko  
337 and Wetherald, 1981) on climate. It is observed that the cloud cover changes in idealized  
338 symmetric continent experiments, i.e. the hemispheric asymmetry in the continental geography  
339 impacts the distribution of cloud cover, measured as the mean of total cloudiness. Cloud cover  
340 affects the climate through two opposing influences; a cooling effect is produced due to  
341 reflection of solar radiation, and a warming effect on climate due to reduction of effective  
342 temperature for outgoing terrestrial (longwave) radiation (Wetherald et al., 1980). However, the  
343 overall effect of increasing cloud cover is generally considered to cause cooling (Manabe et al.,  
344 1967; Schneider, 1972). The hemispheric asymmetry impacts the cloud cover fraction by as  
345 much as 10% at various latitudes (Figure 8a). The effect of asymmetry increases cloudiness over  
346 land poleward of 50° N latitude, contributing to negative net radiation and temperature anomalies  
347 over the Northern Hemisphere continents, and can be observed both in terms of Summer  
348 Temperatures and the PDD. In the Southern Hemisphere, total cloudiness decreases over the  
349 Southern Ocean due to hemispheric asymmetry, contributing to a positive temperature anomaly

350 over this region. At latitudes below 50 degrees, the increase in the area-mean flux of outgoing  
351 terrestrial radiation is almost compensated by the increase in net insolation flux. Thus, we expect  
352 minor impact of cloud content on the LAE at lower latitudes.

353 Snow cover reflects ~80 to 90% of the sun's energy and it has an important influence on energy  
354 balance and regional water budgets. Snow cover's effect on surface energy balance has a strong  
355 cooling effect, and conversely, decreasing snow cover leads to a decrease of surface albedo and  
356 warming. We find that the snow fraction (annual and monthly averages) is also influenced by the  
357 hemispheric asymmetry of the continents. There is a decrease in the snow fraction over most of  
358 Eurasia and North America due to hemispheric asymmetry (Figure 8c), leading to warming in  
359 the asymmetrical Earth when compared to an Earth with symmetric continents. The effect is  
360 more pronounced in the spring months (Figure 8d), which leads to longer summers, increasing  
361 the Positive Degree Days (PDD) in the asymmetric Earth. The relationship between the snow  
362 fraction and temperature anomalies is expected to be weaker in the heavily forested regions (such  
363 as Northern Asia), where the snow-albedo feedback is less effective (Bonan et al., 1992).  
364 Similarly, fractional sea ice cover has an opposing effect on temperature. Thus, an increase in  
365 fractional sea ice cover due to hemispheric asymmetry causes a negative LAE, as increased  
366 albedo reduces net shortwave radiative flux.

367 Spatial patterns in the LAE are compared with basic dynamical effects of the different  
368 geographies. Sea level pressure shows an effect due to hemispheric asymmetry (Figure 8g), with  
369 a general increase in the Northern Hemisphere and a decrease in the Southern Hemisphere. The  
370 resulting change in the time-averaged (mean annual shown here) wind field can be seen in  
371 northward winds (Figure 8h) and imply a dynamical contribution to the LAE anomaly patterns  
372 via warm air advection. Spatial patterns in these dynamical linkages can help explain some of the

373 regional anomalies seen in the LAE. For example, we find reduced winds in the North Atlantic  
374 leading to reduced heat loss out of that region. This hints at a tropical teleconnection to the  
375 westerlies (e.g. Hou, 1998), propagating the impact of low latitude geography to the mid  
376 latitudes of the opposite hemisphere, in this case with an amplifying impact on sea ice and  
377 regional warming in the North Atlantic. We observe a positive relationship between the LAE and  
378 500-hPa geopotential height (Figure 8i), whereby a positive “Z500 effect” indicates that the  
379 geopotential heights are regionally higher (implying warm temperatures across the region) when  
380 compared to a symmetric Earth, and vice-versa. Interhemispheric teleconnections like these have  
381 been studied extensively with respect to present day continental geography (Chiang and  
382 Friedman, 2012; Harnack and Harnack, 1985; Hou, 1998; Ji et al., 2014). However, far field  
383 effects such as those arising from interactions between the Hadley circulation and planetary  
384 waves (among other dynamical processes) are not adequately resolved at the relatively coarse  
385 spatial resolution used in these initial simulations, with monthly meteorological output. A more  
386 complete dynamical analysis of the LAE is the subject of ongoing work and a future manuscript.

## 387 **7. Conclusions**

388 The unbalanced fraction of land in the Northern versus Southern Hemisphere has remained  
389 almost unchanged for tens of millions of years. However, the significance of this continental  
390 asymmetry on Earth’s climate response to forcing has not been previously quantified with a  
391 physically based climate models. We find that continental geography of the opposite hemisphere  
392 has a control on the climate system’s response to insolation forcing, and this may help explain  
393 the non-linear response of the Earth’s climate to insolation forcing.

394 According to classical Milankovitch theory, the growth of polar ice sheets at the onset of  
395 glaciation requires cooler summers in the high latitudes, in order for snow to persist throughout

396 the year. During warm summers at the high latitudes, the winter snowpack melts, inhibiting  
397 glaciation or leading to deglaciation if ice sheets already exist. Thus, the intensity of summer  
398 insolation at high latitudes, especially the Northern polar latitudes, has been considered the key  
399 driver of the glacial-interglacial cycles and other long-term climatic variations. At precessional  
400 periods, at which the high latitude summer insolation intensity primarily varies (Huybers, 2006;  
401 Raymo et al., 2006, etc.), the land asymmetry effect plays an important role by amplifying (and  
402 weakening at certain times) the effect of summer insolation intensity.

403 In all the orbital configurations simulated here, we find that the geography of the Southern  
404 Hemisphere weakens the temperature response of the high Northern Hemisphere latitudes to  
405 orbital forcing. Consequently, this leads to a larger latitudinal gradient in summer temperatures  
406 in the Northern Hemisphere compared to that of a symmetric Earth. In particular, the  
407 amplification (or weakening) of the response to insolation changes at precessional and obliquity  
408 periods might explain some of the important features of late Pliocene-early Pleistocene climate  
409 variability, when obliquity-paced cyclicity dominated precession in global benthic  $\delta^{18}\text{O}$  records.  
410 In Figure 7, we have demonstrated that the interhemispheric effect causes a suppression of the  
411 effects of precessional cycle on the Earth's surface. In other words, the real Earth has a smaller  
412 response to a precession cycle as compared to the hypothetical symmetric Earth. We have also  
413 showed that the interhemispheric effect causes an amplification of the effects of obliquity cycle  
414 on the Earth's surface. In other words, the real Earth has a larger response to the obliquity cycle  
415 in the ocean dominated Southern Hemisphere, as compared to the hypothetical symmetric Earth.  
416 Consequently, the interhemispheric effect of continental geography contributes to the muting of  
417 precessional signal and amplification of obliquity signal recorded in paleoclimate proxies such as  
418 benthic  $\delta^{18}\text{O}$  isotope records.

419 There are various ways in which the Earth's continental asymmetry affects climate. Here, we  
420 have shown how these interhemispheric effects influence the Earth's climate response to orbital  
421 forcing via the radiative and atmospheric dynamical processes represented in a slab-ocean GCM.  
422 While computationally challenging, future work should include complimentary simulations with  
423 AOGCMs, to explore the potential modifying role of ocean dynamics on the amplifying and  
424 weakening interhemispheric responses to orbital forcing demonstrated here.



425 **Table 1. Experimental Setup of Model Boundary Conditions and Forcings**

| Run ID                     | LSX Configuration | Eccentricity | Obliquity | Precession <sup>a</sup> | GHGs          |
|----------------------------|-------------------|--------------|-----------|-------------------------|---------------|
| CONTROL <sub>NHSP</sub>    | Modern            | 0.034        | 23.2735   | 270° (NHSP)             | Preindustrial |
| CONTROL <sub>SHSP</sub>    | Modern            | 0.034        | 23.2735   | 90° (SHSP)              | Preindustrial |
| CONTROL <sub>EP1</sub>     | Modern            | 0.034        | 23.2735   | 0° (EP1)                | Preindustrial |
| CONTROL <sub>EP2</sub>     | Modern            | 0.034        | 23.2735   | 180° (EP2)              | Preindustrial |
| CONTROL <sub>HIGH</sub>    | Modern            | 0.034        | 24.5044   | 180°                    | Preindustrial |
| CONTROL <sub>LOW</sub>     | Modern            | 0.034        | 22.0425   | 180°                    | Preindustrial |
|                            |                   |              |           |                         |               |
| NORTH-SYMM <sub>NHSP</sub> | North-symmetric   | 0.034        | 23.2735   | 270° (NHSP)             | Preindustrial |
| NORTH-SYMM <sub>SHSP</sub> | North-symmetric   | 0.034        | 23.2735   | 90° (SHSP)              | Preindustrial |
| NORTH-SYMM <sub>EP1</sub>  | North-symmetric   | 0.034        | 23.2735   | 0° (EP1)                | Preindustrial |
| NORTH-SYMM <sub>EP2</sub>  | North-symmetric   | 0.034        | 23.2735   | 180° (EP2)              | Preindustrial |
| NORTH-SYMM <sub>HIGH</sub> | North-symmetric   | 0.034        | 24.5044   | 180°                    | Preindustrial |
| NORTH-SYMM <sub>LOW</sub>  | North-symmetric   | 0.034        | 22.0425   | 180°                    | Preindustrial |
|                            |                   |              |           |                         |               |
| SOUTH-SYMM <sub>NHSP</sub> | South-symmetric   | 0.034        | 23.2735   | 270° (NHSP)             | Preindustrial |
| SOUTH-SYMM <sub>SHSP</sub> | South-symmetric   | 0.034        | 23.2735   | 90° (SHSP)              | Preindustrial |
| SOUTH-SYMM <sub>EP1</sub>  | South-symmetric   | 0.034        | 23.2735   | 0° (EP1)                | Preindustrial |
| SOUTH-SYMM <sub>EP2</sub>  | South-symmetric   | 0.034        | 23.2735   | 180° (EP2)              | Preindustrial |
| SOUTH-SYMM <sub>HIGH</sub> | South-symmetric   | 0.034        | 24.5044   | 180°                    | Preindustrial |
| SOUTH-SYMM <sub>LOW</sub>  | South-symmetric   | 0.034        | 22.0425   | 180°                    | Preindustrial |

426 **NHSP:** Northern Hemisphere Summer Solstice at Perihelion

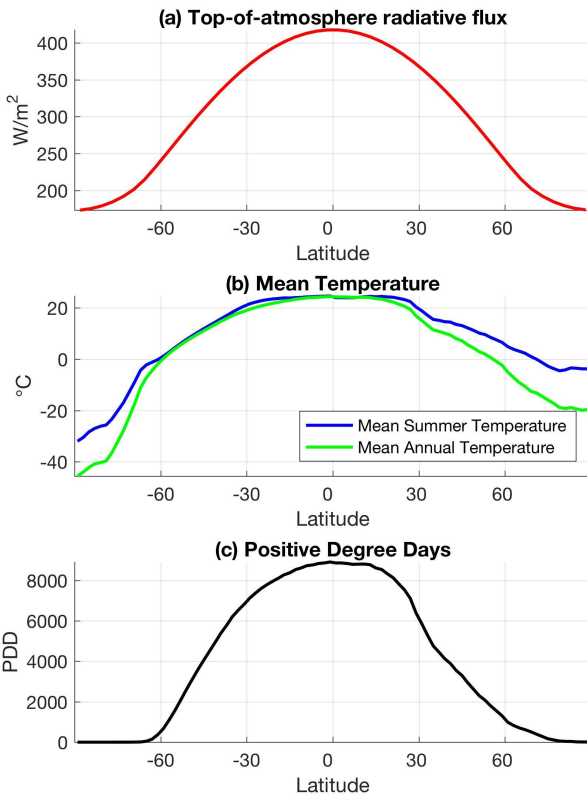
427 **SHSP:** Southern Hemisphere Summer Solstice at Perihelion

428 **EP1:** Northern Hemisphere Vernal Equinox at Perihelion

429 **EP2:** Northern Hemisphere Autumnal Equinox at Perihelion

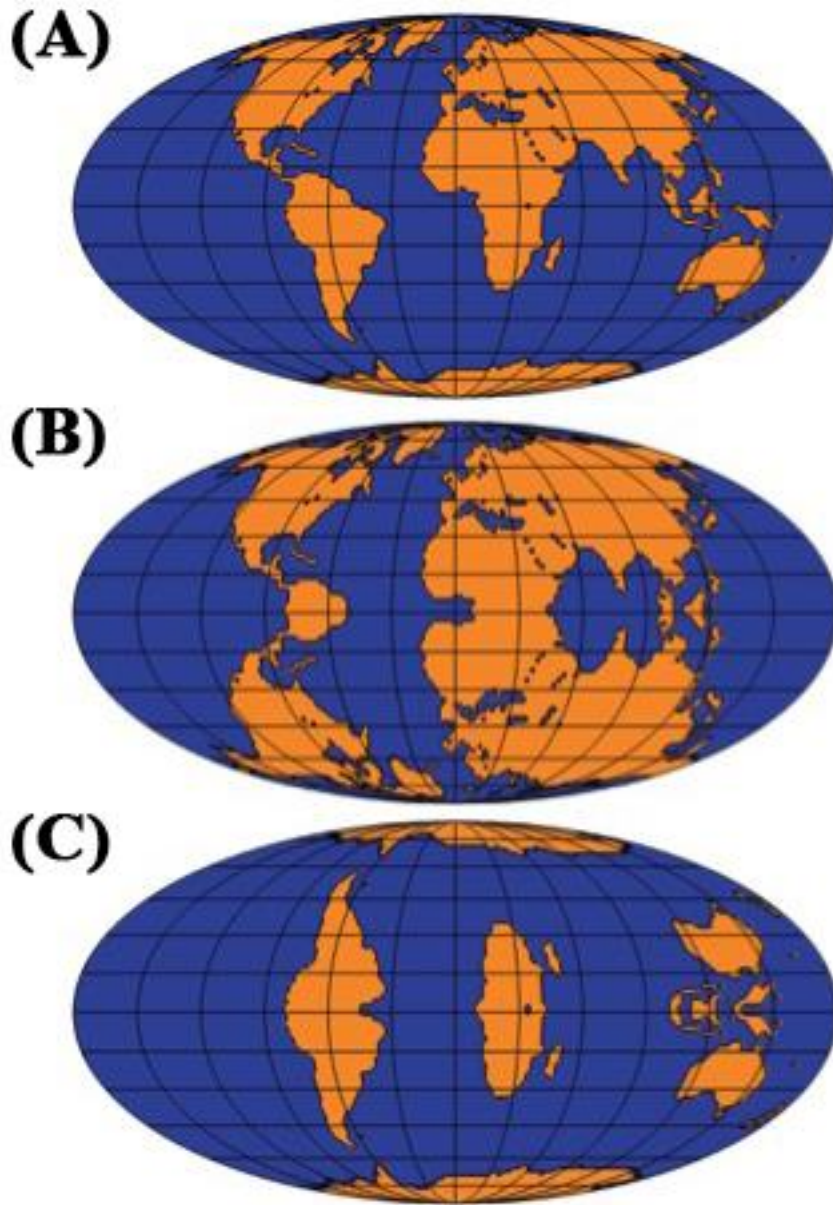
430 <sup>a</sup> Orbital precession in the GCM is defined here as the prograde angle from perihelion to the

431 Northern Hemispheric vernal equinox.



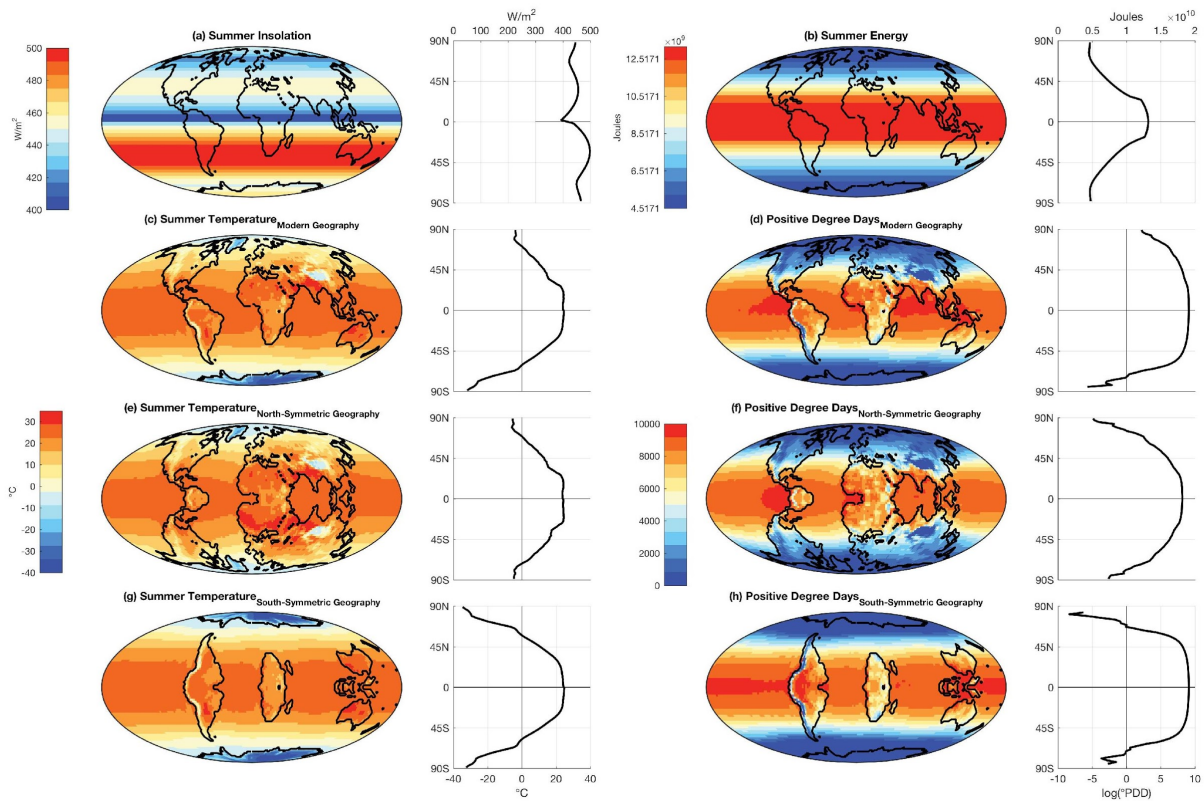
432

433 **Figure 1:** (a) Top-of-atmosphere net incoming radiation (red). (b) Mean Summer Temperatures  
 434 (blue) and Mean Annual Temperatures (green), computer from GCM simulations with a modern  
 435 orbit (c) Positive Degree Days (PDD) calculated from GCM simulations with a modern orbit.



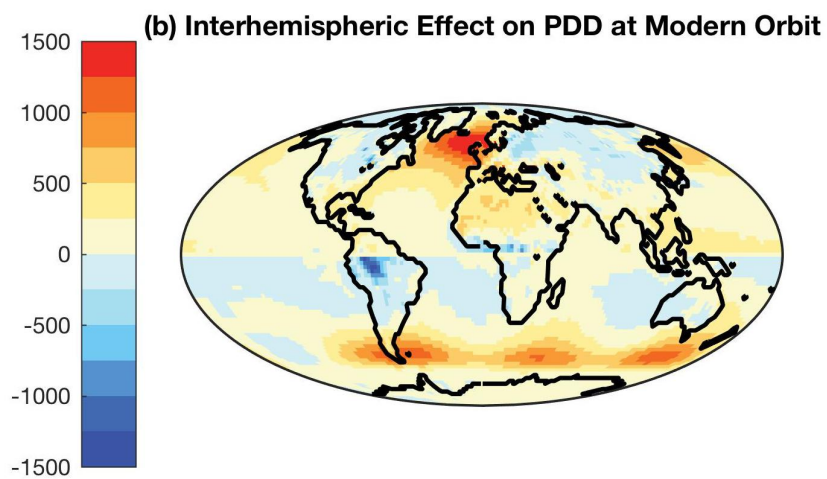
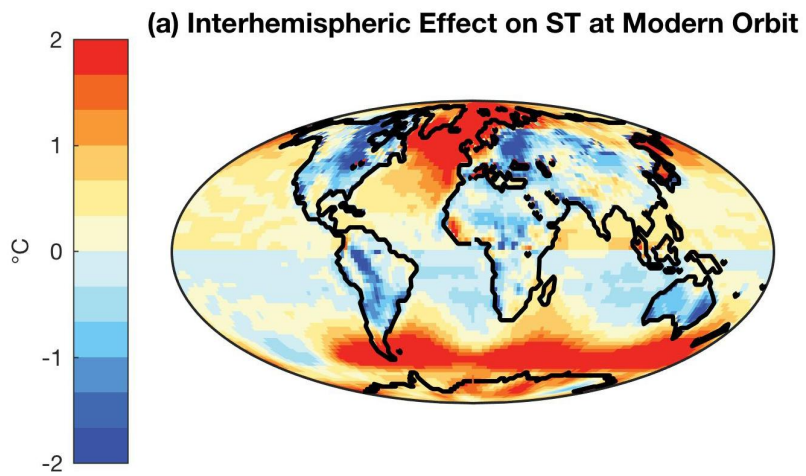
436

437 **Figure 2:** (A) Modern continental geography (B) NORTH-SYMM geography and (C) SOUTH-  
438 SYMM geography



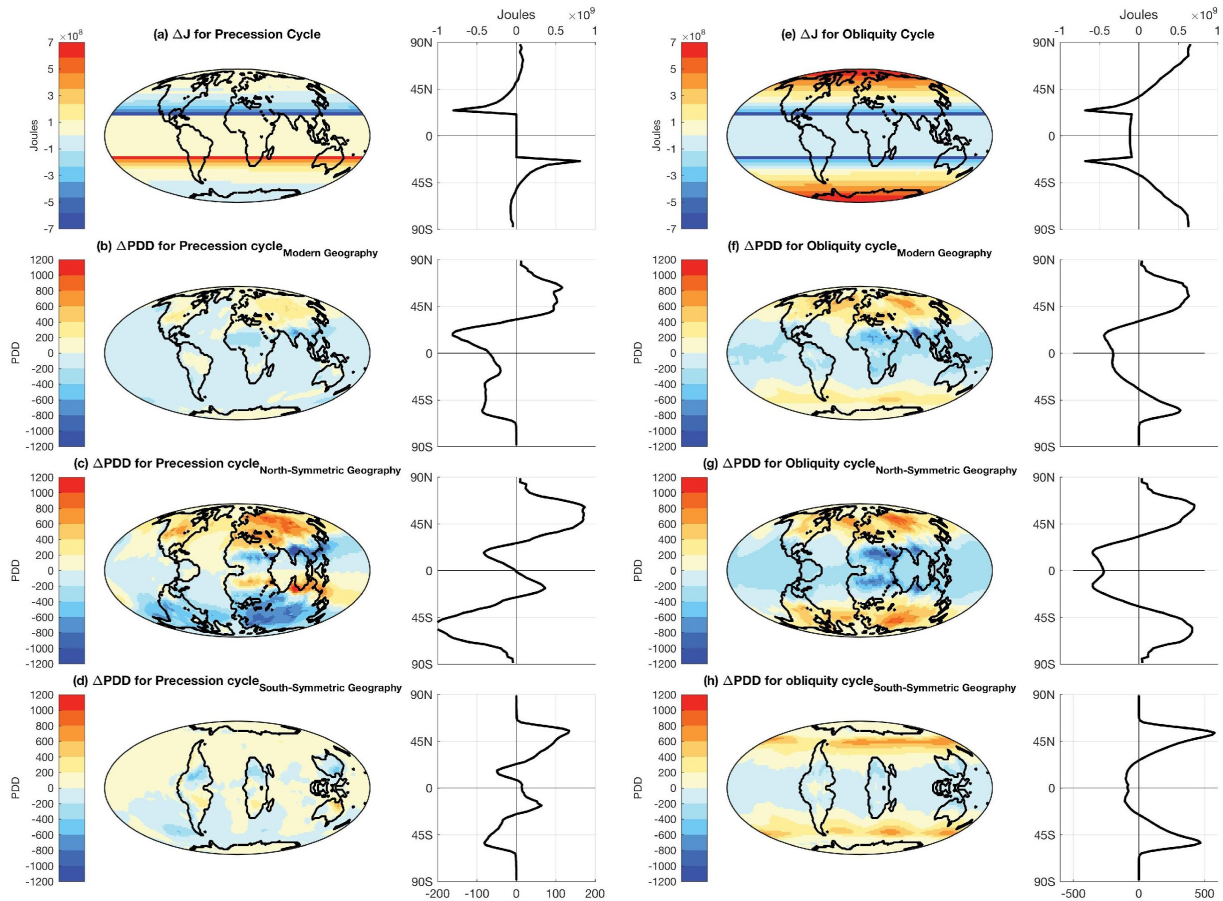
439

440 **Figure 3:** (a-d) Demonstration of Earth's asymmetric climate response to symmetric climate  
 441 forcing. Simulations are forced with modern orbit: (a) Summer insolation; (b) summer energy;  
 442 (c) Summer Temperature; and (d) PDD. (e-h) Demonstration of Earth's symmetric climate  
 443 response to climate forcing when idealized symmetric Earth geographies are used. Simulations  
 444 are forced by modern day orbit: (e) and (f) Summer Temperature and PDD for NORTH-SYMM  
 445 simulation, (g) and (h) Summer Temperature and PDD for SOUTH-SYMM simulation. The  
 446 zonal averages are plotted on the right of each Figure. Zonal averages of PDD are plotted on a  
 447 log scale.



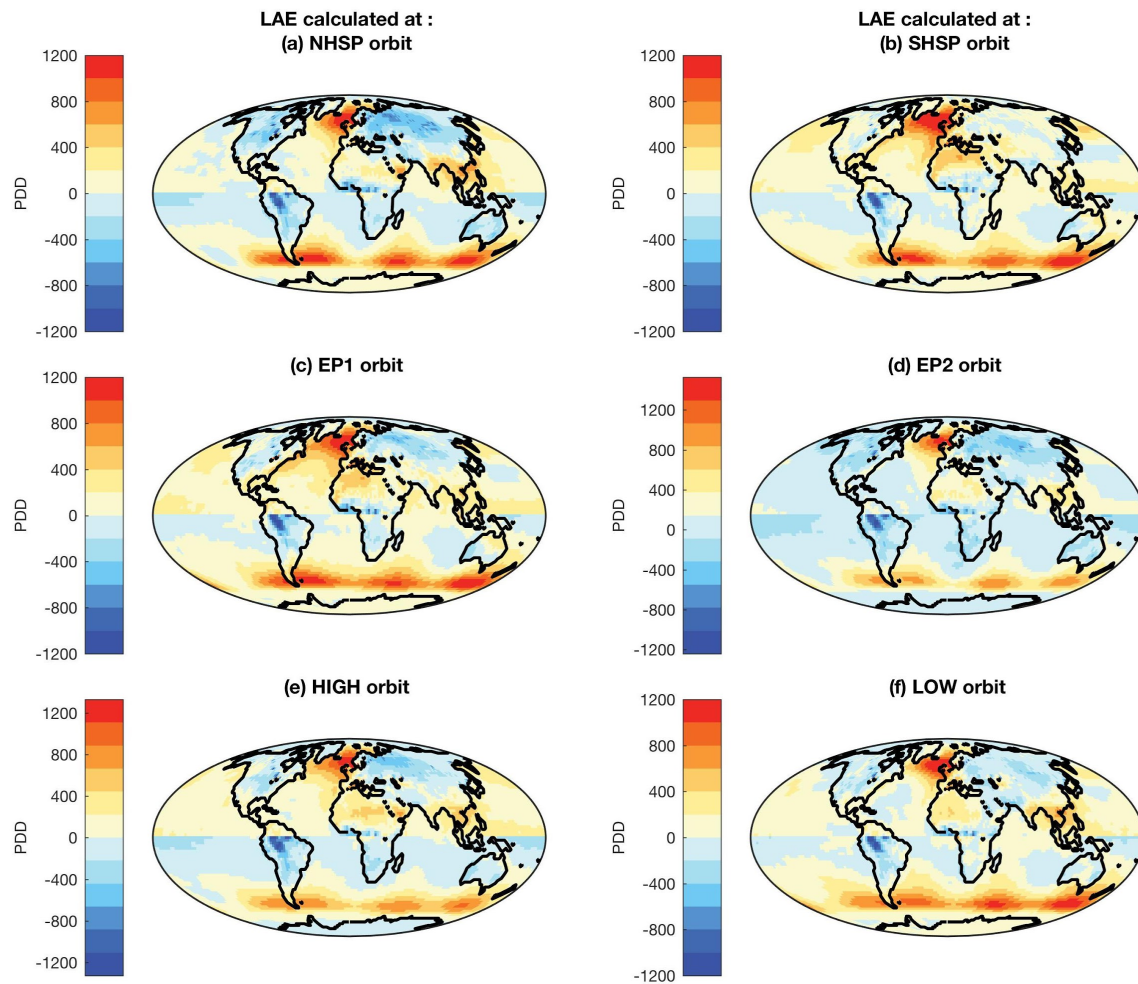
448

449 **Figure 4:** Interhemispheric effect of continental geography (LAE) on: (a) Mean Summer  
450 Temperature (ST) and (b) Positive Degree Days (PDD).



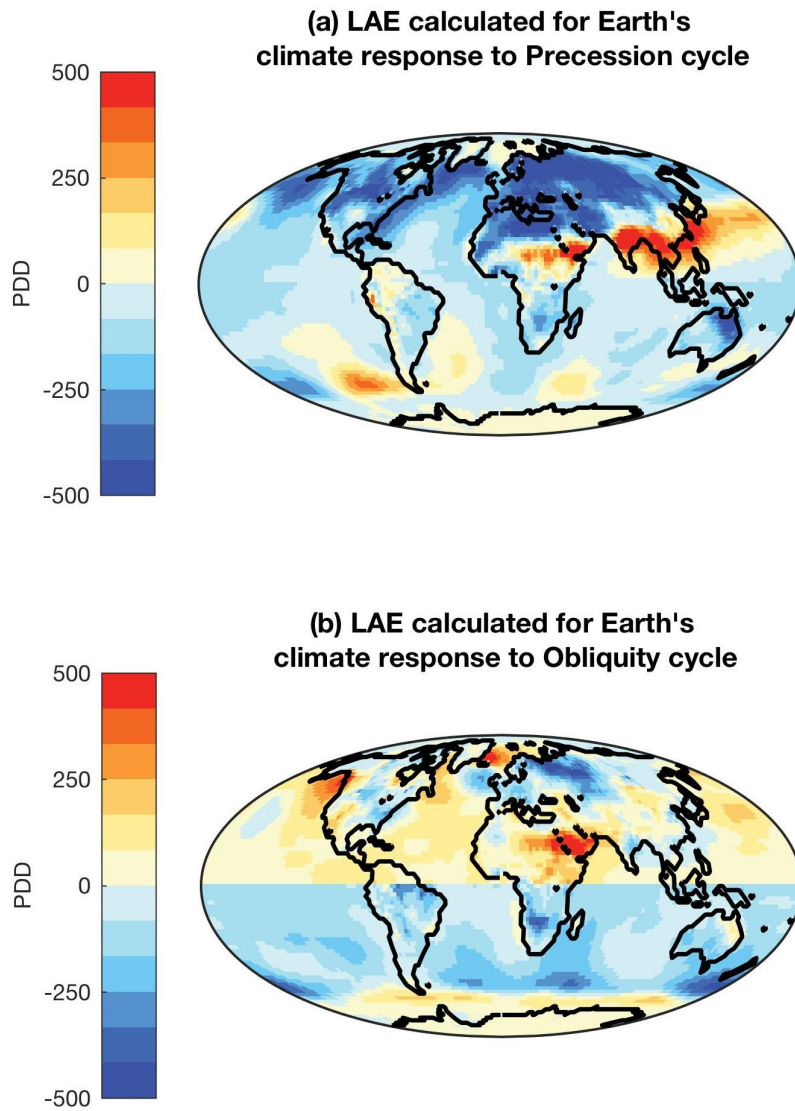
451

452 **Figure 5:** Summer Energy (J) change for a transition from SHSP to NHSP orbit (a); and the  
 453 corresponding change in Positive Degree Days (PDD) in CONTROL (b); NORTH-SYMM (c)  
 454 and SOUTH-SYMM (d) simulations. Summer Energy (J) change for a transition from LOW to  
 455 HIGH orbit (e); and the corresponding change in PDD in CONTROL (f); NORTH-SYMM (g)  
 456 and SOUTH-SYMM (h) simulations.



457

458 **Figure 6:** Interhemispheric effect of continental geography (LAE) on the climate response  
 459 (PDD) at: (a) Northern Hemisphere summer at perihelion; (b) Southern Hemisphere summer at  
 460 perihelion; (c) Northern Hemisphere vernal equinox at perihelion; (d) Northern Hemisphere  
 461 autumnal equinox at perihelion; (e) High obliquity orbit; and (f) Low obliquity orbit.

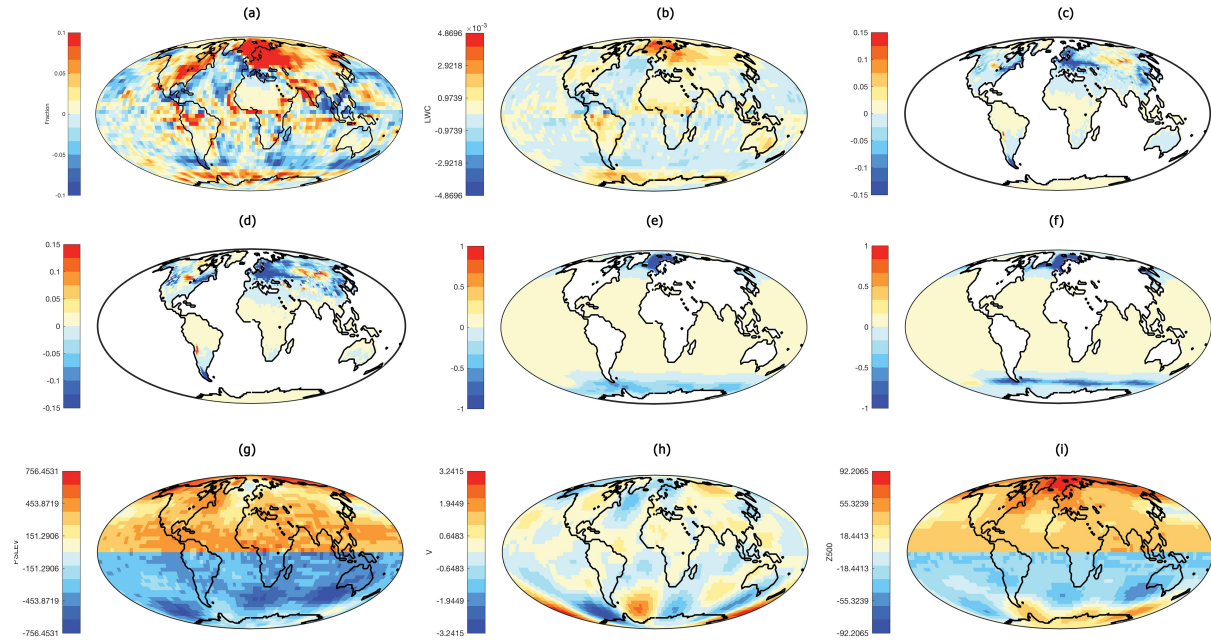


462

463 **Figure 7:** Interhemispheric effect of continental geography on the climate response to: (a)

464 precession cycle (SHSP to NHSP); and (b) obliquity cycle (Low to High).





465

466 **Figure 8:** The effect of interhemispheric continental distribution on: (a) Mean annual cloud  
 467 cover fraction (b) Liquid water content from all cloud types (kg/kg) (c) Fractional snow cover  
 468 (annual mean) (d) Fractional snow cover (averaged over spring months) (e) Fractional sea ice  
 469 cover (annual mean) (f) Fractional sea ice cover (averaged over spring months) (g) Sea level  
 470 pressure (Pa, annual mean) (h) Northward wind (m/s, annual mean) (i) 500 hPa geopotential  
 471 height (m, annual mean).

472

473 Alder, J. R., Hostetler, S. W., Pollard, D. and Schmittner, A.: Evaluation of a present-day climate  
474 simulation with a new coupled atmosphere-ocean model GENMOM, *Geosci. Model Dev.*, 4(1),  
475 69–83, doi:10.5194/gmd-4-69-2011, 2011.

476 Barron, E. J., Thompson, S. L. and Hay, W. W.: Continental distribution as a forcing factor for  
477 global-scale temperature, *Nature*, 310(5978), 574–575, doi:10.1038/310574a0, 1984.

478 Berger, A. and Loutre, M. F.: Insolation values for the climate of the last 10 million years, *Quat.*  
479 *Sci. Rev.*, 10(4), 297–317, doi:10.1016/0277-3791(91)90033-Q, 1991.

480 Bonan, G. B., Pollard, D. and Thompson, S. L.: Effects of boreal forest vegetation on global  
481 climate, *Nature*, 359(6397), 716–718, doi:10.1038/359716a0, 1992.

482 Charles Lyell: *Principles of Geology*, John Murray: Albemarle Street, London. [online]  
483 Available from: <https://www.bl.uk/collection-items/charles-lyells-principles-of-geology#>  
484 (Accessed 31 January 2018), 1832.

485 Chiang, J. C. H. and Friedman, A. R.: Extratropical Cooling, Interhemispheric Thermal  
486 Gradients, and Tropical Climate Change, *Annu. Rev. Earth Planet. Sci.*, 40(1), 383–412,  
487 doi:10.1146/annurev-earth-042711-105545, 2012.

488 Croll, J.: On ocean-currents, part I: ocean-currents in relation to the distribution of heat over the  
489 globe., *Philos. Mag. J. Sci.*, 39(259), 81–106, 1870.

490 Deconto, R. M., Pollard, D., Wilson, P. A., Pälike, H., Lear, C. H. and Pagani, M.: Thresholds  
491 for Cenozoic bipolar glaciation., *Nature*, 455(7213), 652–6, doi:10.1038/nature07337, 2008.

492 Flato, G. M. and Boer, G. J.: Warming asymmetry in climate change simulations, *Geophys. Res.*  
493 *Lett.*, 28(1), 195–198, doi:10.1029/2000GL012121, 2001.

494 Harnack, R. P. and Harnack, J.: Intra- and inter-hemispheric teleconnections using seasonal  
495 southern hemisphere sea level pressure, *J. Climatol.*, 5(3), 283–296,  
496 doi:10.1002/joc.3370050305, 1985.

497 Hay, W. W., Barron, E. J. and Thompson, S. L.: Results of global atmospheric circulation  
498 experiments on an Earth with a meridional pole-to- pole continent, *J. Geol. Soc. London.*,  
499 147(2), 385–392, doi:10.1144/gsjgs.147.2.0385, 1990.

500 Hou, A. Y.: Hadley Circulation as a Modulator of the Extratropical Climate, *J. Atmos. Sci.*,  
501 55(14), 2437–2457, doi:10.1175/1520-0469(1998)055<2437:HCAAMO>2.0.CO;2, 1998.

502 Huybers, P.: Early Pleistocene glacial cycles and the integrated summer insolation forcing.,  
503 *Science*, 313(5786), 508–11, doi:10.1126/science.1125249, 2006.

504 Ji, X., Neelin, J. D., Lee, S.-K., Mechoso, C. R., Ji, X., Neelin, J. D., Lee, S.-K. and Mechoso, C.  
505 R.: Interhemispheric Teleconnections from Tropical Heat Sources in Intermediate and Simple  
506 Models, *J. Clim.*, 27(2), 684–697, doi:10.1175/JCLI-D-13-00017.1, 2014.

507 Kang, S. M., Seager, R., Frierson, D. M. W. and Liu, X.: Croll revisited: Why is the northern  
508 hemisphere warmer than the southern hemisphere?, *Clim. Dyn.*, doi:10.1007/s00382-014-2147-z,  
509 2014.

510 Kiehl, J. T., Hack, J. J., Bonan, G. B., Boville, B. a., Williamson, D. L. and Rasch, P. J.: The  
511 National Center for Atmospheric Research Community Climate Model: CCM3\*, *J. Clim.*, 11(6),

512 1131–1149, doi:10.1175/1520-0442(1998)011<1131:TNCFAR>2.0.CO;2, 1998.

513 Koenig, S. J., DeConto, R. M. and Pollard, D.: Pliocene Model Intercomparison Project  
514 Experiment 1: implementation strategy and mid-Pliocene global climatology using GENESIS  
515 v3.0 GCM, *Geosci. Model Dev.*, 5(1), 73–85, doi:10.5194/gmd-5-73-2012, 2012.

516 Loutre, M.-F., Paillard, D., Vimeux, F. and Cortijo, E.: Does mean annual insolation have the  
517 potential to change the climate?, *Earth Planet. Sci. Lett.*, 221(1–4), 1–14, doi:10.1016/S0012-  
518 821X(04)00108-6, 2004.

519 Manabe, S., Wetherald, R. T., Manabe, S. and Wetherald, R. T.: Thermal Equilibrium of the  
520 Atmosphere with a Given Distribution of Relative Humidity, *J. Atmos. Sci.*, 24(3), 241–259,  
521 doi:10.1175/1520-0469(1967)024<0241:TEOTAW>2.0.CO;2, 1967.

522 Meleshko, V. P. and Wetherald, R. T.: The effect of a geographical cloud distribution on climate:  
523 A numerical experiment with an atmospheric general circulation model, *J. Geophys. Res.*,  
524 86(C12), 11995, doi:10.1029/JC086iC12p11995, 1981.

525 Philander, S. G. H., Gu, D., Lambert, G., Li, T., Halpern, D., Lau, N.-C. and Pacanowski, R. C.:  
526 Why the ITCZ Is Mostly North of the Equator, *J. Clim.*, 9(12), 2958–2972, doi:10.1175/1520-  
527 0442(1996)009<2958:WTIIMN>2.0.CO;2, 1996.

528 Raymo, M. E., Lisiecki, L. E. and Nisancioglu, K. H.: Plio-Pleistocene Ice Volume, Antarctic  
529 Climate, and the Global  $\delta^{18}\text{O}$  Record, , 313(July), 492–495, 2006.

530 Robinson, D. A., Dewey, K. F., Heim, R. R., Robinson, D. A., Dewey, K. F. and Richard R.  
531 Heim, J.: Global Snow Cover Monitoring: An Update, *Bull. Am. Meteorol. Soc.*, 74(9), 1689–

532 1696, doi:10.1175/1520-0477(1993)074<1689:GSCMAU>2.0.CO;2, 1993.

533 Schneider, S. H.: Cloudiness as a Global Climatic Feedback Mechanism: The Effects on the  
534 Radiation Balance and Surface Temperature of Variations in Cloudiness, *J. Atmos. Sci.*, 29(8),  
535 1413–1422, doi:10.1175/1520-0469(1972)029<1413:CAAGCF>2.0.CO;2, 1972.

536 Short, D. A., Mengel, J. G., Crowley, T. J., Hyde, W. T. and North, G. R.: Filtering of  
537 Milankovitch Cycles by Earth's Geography, *Quat. Res.*, 35(02), 157–173, doi:10.1016/0033-  
538 5894(91)90064-C, 1991.

539 Stone, P. H.: Constraints on dynamical transports of energy on a spherical planet, *Dyn. Atmos.*  
540 *Ocean.*, 2(2), 123–139, doi:10.1016/0377-0265(78)90006-4, 1978.

541 Stouffer, R. J., Manabe, S. and Bryan, K.: Interhemispheric asymmetry in climate response to a  
542 gradual increase of atmospheric CO<sub>2</sub>, *Nature*, 342(6250), 660–662, doi:10.1038/342660a0,  
543 1989.

544 Thompson, S. L. and Pollard, D.: Greenland and Antarctic Mass Balances for Present and  
545 Doubled Atmospheric CO<sub>2</sub> from the GENESIS Version-2 Global Climate Model, *J. Clim.*,  
546 10(5), 871–900, doi:10.1175/1520-0442(1997)010<0871:GAAMBF>2.0.CO;2, 1997.

547 Trenberth, K. E., Fasullo, J. T., Kiehl, J., Trenberth, K. E., Fasullo, J. T. and Kiehl, J.: Earth's  
548 Global Energy Budget, *Bull. Am. Meteorol. Soc.*, 90(3), 311–323,  
549 doi:10.1175/2008BAMS2634.1, 2009.

550 Wetherald, R. T., Manabe, S., Wetherald, R. T. and Manabe, S.: Cloud Cover and Climate  
551 Sensitivity, *J. Atmos. Sci.*, 37(7), 1485–1510, doi:10.1175/1520-

552 0469(1980)037<1485:CCACS>2.0.CO;2, 1980.

553